Highly Electrically Conductive Ag-Doped Graphene Fibers as Stretchable Conductors

*Zhen Xu, Zheng Liu, Haiyan Sun, and Chao Gao**

Graphene has emerged as a paradigmatic 2D carboneous nanomaterial and attracted considerable attentions because of its outstanding electrical, thermal, and mechanical merits.[1–5] Descending from the first micromechanical exfoliation of graphene,[6] the scalable synthesis of highly soluble graphene sheets as ultrathin building blocks, representatively exemplified by graphene oxide (GO) or chemically reduced graphene (CRG), has promoted the fabrication of graphene-based macroscopic materials, by simple but effective fluid assembly approaches.[7–22] These efforts involved the wet-spinning assembly of continuous graphene fibers from GO liquid crystals,[12–17] the hydrothermal or ice-templated assembly for graphene aerogel and 3D frameworks,[18–21] and filtration-assisted assembly of large area graphene film/papers.[22,23] The versatile macroscopic-assembled graphene materials possessed the outstanding properties of graphene, such as high mechanical strength, fine electrical conductivity and high specific surface area, and are poised to be widely applicable in high-performance materials, chemical supercapacitors, ultralight aerogels, sensors and catalysts.

In the family of graphene-based macroscopic materials, graphene fibers are of special significance, from which multidimensional, versatile graphene-based materials (such as bulk plates and textiles) and devices (for example stretchable supercapacitors) can be readily accessed. Three aspects are crucial to further the practical application of graphene fibers, including mechanical performance, electrical conductivity, and thermal conductivity. Since the first spinning of graphene fibers from graphene-based liquid crystals,[12] considerable efforts have been devoted to improve their mechanical strength, such as the choice of giant sizes of graphene sheets, the introduction of divalent ions crosslinking and the optimization of the spinning process.[14,17] However, graphene fibers still showed limited electrical conductivity (4.1×10^4 S/m), mainly due to their structural defects and oxygen-containing groups in constituent CRG sheets.[7–11] To meet the wide use of graphene fibers as lightweight conductors, wearable electronics, and actual microcables, their electrical conductivity is needed to be considerably improved.

In this paper, we focused on the improvement of electrically conductivity of graphene fibers. For the first time, we prepared continuous graphene-metal hybrid fibers by wet-spinning of giant graphene oxide (GGO) liquid crystals mixed with commercial Ag nanowires (NWs), followed by chemical reduction. The Ag-doped graphene fibers possess the record high electrical conductivity up to 9.3×10^4 S/m and high current capacity of 7.1×10^3 A/cm^2, with 330% and 1500% enhancement factor, respectively. Depending on the choice of chemical reduction method, the conductivity of graphene fibers show molecular doping mechanism in HI reduction and mixing mechanism in mild vitamin C (VC) reduction. The combination of high conductivity and high mechanical strength and fine flexibility of doped graphene fibers renders them good stretchable conductors to be applied in soft circuits.

Wet-Spinning of GGO-Ag NW Fibers: We prepared GGO sheets by modified Hummers' method,[24] as described in our previous report[14] and in the Supporting Information. The average lateral size of the GGO sheets is calculated as being about 20 μm from their SEM inspections and the representative thickness is measured as 0.8 nm in the AFM images (**Figure 1**A and Supporting Information, Figure S1). The lateral giant size and the atomic thickness of the GGO sheets facilitate the formation of liquid crystals in their good solvents, such as extensively investigated water,[25–29] N,N-dimethylformamide (DMF) and N-methyl-2-pyrrolidone (NMP), especially at relatively low concentrations down to 2 mg/mL (Supporting Information, Figure S2). The introduction of Ag NWs shows negligible influence to the liquid crystalline behavior of GGO sheets in DMF, as shown in the polarized optical microscopy (POM) image of a GGO mixture dispersion at 4 mg/mL (Figure 1D), with a Ag NW weight percentage of 5%. The presence of GGO sheets increases the dispersibility of Ag NW, and the mixture of GGO and Ag NWs shows no precipitation after long-time rest (for example one month as shown in Figure 1E), contrary to the precipitation in the pure Ag NW dispersions just after 12 h rest despite of the protection of polyvinylpyrrolidone (PVP) ligand (Supporting Information, Figure S3). In the optical image of GGO-Ag NWs mixture loaded in the planar cell (Figure 1E), random distribution of Ag NWs was seen under the rest state.

Followed by the spinning process to make GGO-Ag NWs fiber using the homemade spinning apparatus (Supporting Information, Figure S4), we can obtain continuous GGO-Ag NWs hybrid fibers with length up to 100 m (**Figure 2**A,B). The flow field in the spinning tubes not only favors the more ordered structure of GGO sheets in the gel fiber, but also improves the alignment of Ag NWs along the fiber axis. The POM image of the coagulated gel fiber in Figure 1F shows more distinct and uniform nematic textures than the spinning dopes in the planar cell, suggesting the more regular alignment of GGO sheets after unidirectional flow. Simultaneously, the Ag NWs in the gel fiber shows highly regular alignment along the

Z. Xu, Z. Liu, H. Y. Sun, Prof. C. Gao
MOE Key Laboratory of Macromolecular Synthesis and Functionalization
Department of Polymer Science and Engineering
Zhejiang University
38 Zheda Road, Hangzhou 310027, P. R. China
E-mail: chaogao@zju.edu.cn

DOI:10. 1002/adma.201300774

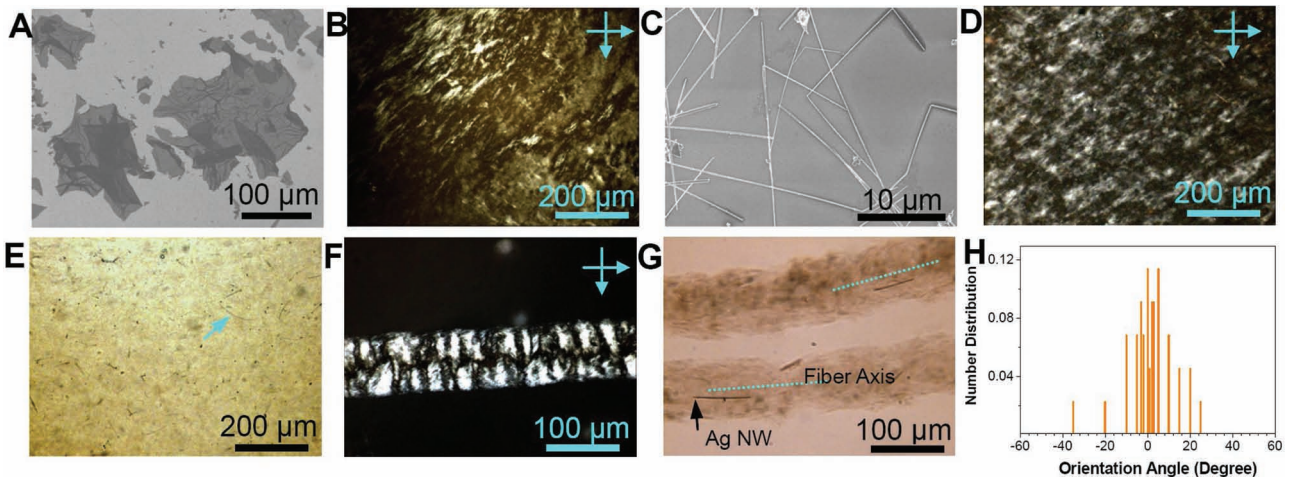

Figure 1. A) SEM image of GGO sheets deposited on silica. B) POM image of GGO DMF dispersion (4 mg/mL) between crossed polarizers. C) SEM image of commercial Ag nanowires. D,E) POM image of GGO-Ag NWs dispersions between crossed polarizers in the planar cell (D) and the corresponding optical image under natural light (E). F,G) POM image between crossed polarizers (F) and optical image under natural light (G) of GGO-Ag NWs gel fibers. The arrow in (E) indicates a Ag nanowire and the dashed lines in (G) represent the gel fiber axis. H) The orientation-angle distribution of Ag NWs along the fiber axis in the gel fibers. The data were calculated from the optical images of GGO-Ag NWs fibers in Figure S5 in the Supporting Information.

fiber axis (Figure 1G and Supporting Information, Figure S5), and the distribution of orientation angle between Ag NWs and fiber axis has a peak in the range of –20–20° (Figure 1H), with an average orientation angle of ±7.3°. This flow-induced alignment phenomenon has been observed in our previous reports for spinning neat graphene fibers[13,14] and the experiments to fabricate aligned CNT arrays on the substrates.[30]

The Structure of GGO-Ag NW Fibers: After air-drying at 60 ° C, the coagulated gel fibers with an average diameter about 100 μm contracted to thin solid fibers with a typical diameter of 10 μm. The surface of a fiber of the solid GGO-Ag NWs shows banded wrinkles parallel to the fiber axis, resembling the dehydration-induced folding behavior in GO membranes dried from aqueous dispersions on substrates.[29] The uniform alignment of wrinkles is mainly caused by the shrinkage in the single radical dimension of fibers.[13–15] In the dried GGO-Ag NW fibers, the regularly aligned asymmetrical building blocks are the GGO sheets and the Ag NWs, inheriting from their alignment in the gel fibers. As shown in Figure 2b, the section morphology of GGO-Ag NWs fiber shows a compact origami-flower-like structure with dentate bends, which is very similar to the section structures of neat GGO fibers.[13–15] These dentate bends with regular lamellar local regions could originate from the orientation disclinations in the liquid crystalline gels. Furthermore, the head face of Ag NWs can be identified in the fiber section, suggesting the alignment of the nanowires along the fiber axis. Energy-dispersive spectroscopy (EDS) mapping images of the fiber section in Figure 2c–f confirmed the existence of C, O,

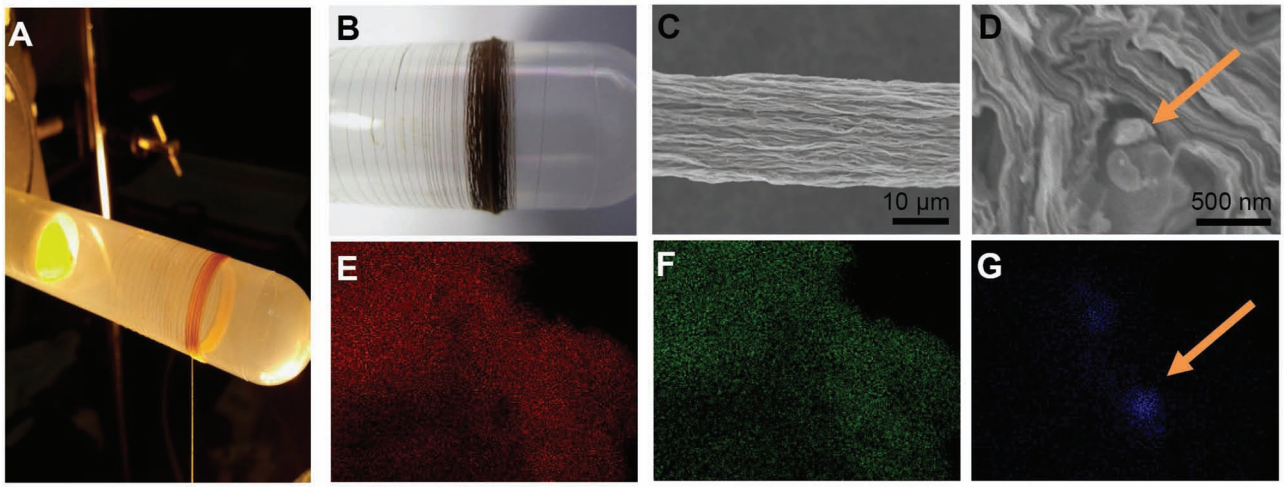

Figure 2. A,B) Digital photos of GGO-Ag NWs fibers collected on a plastic drum during the spinning process (A) and the prepared dried fibers with the length up to 100 m (B). C,D) SEM images of the GGO-Ag NWs fiber surface (C) and the section morphology (D). The arrow in (D) denotes the section of interior Ag NWs. E,F) Carbon (E), oxygen (F) and Ag (G) EDS mapping images in the area of (D). The arrow in (G) indicates the Ag NWs as seen in (D).

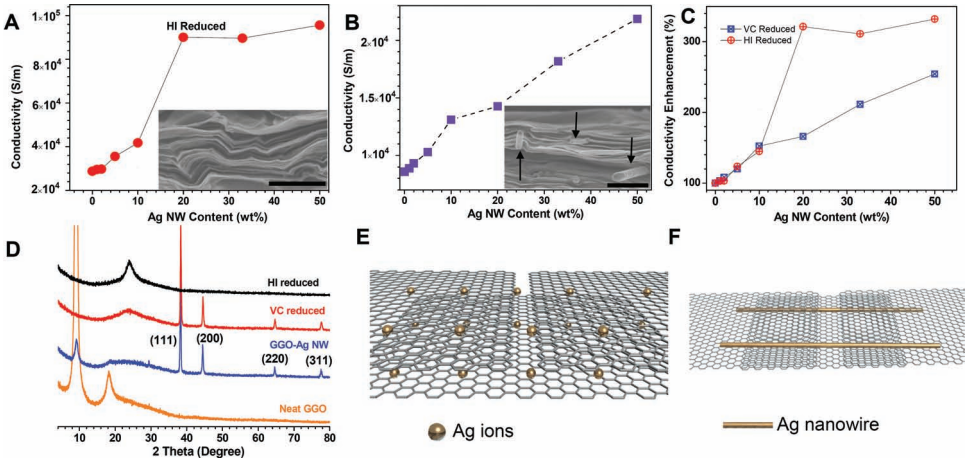

Figure 3. A,B) Plots of electrical conductivities as a function of feed Ag NWs weight percentage in original GGO-Ag NWs fibers reduced by HI (A) and VC (B). The inserted SEM images are the section morphologies of HI-reduced (A) and VC-reduced RGG-Ag composites, respectively. The scale bars in A and B are 1 μm and the arrows in B indicate the Ag NWs. C) The enhancement factor in electrical conductivities of reduced RGG-Ag fibers as a function of the feed Ag NWs weight percentage in original GGO-Ag NWs fibers. D) XRD patterns of neat GGO fibers, GGO-Ag NWs fibers, and RGG-Ag fibers reduced by HI and VC. E,F) Schematic images of the molecular doping mechanism by Ag ions in HI-reduced RGG-Ag fibers (E) and complex mechanism by Ag NWs in VC-reduced RGG-Ag fibers (F).

and Ag elements (the EDS spectra and the elements contained see Figure S6 in the Supporting Information) and the Ag-element mapping image (Figure 2f) agreed with the distribution of Ag NWs observed in the section morphology (Figure 2b).

The Electrical Conductivity and Current Capacity of Graphene-Ag Fibers: In this study, we chose two typical reduction methods by HI and VC to prepare reduced giant graphene (RGG)-Ag fibers.[14,31–33] For the chemical reaction between metallic Ag and HI, the Ag NWs dissolve in HI to form Ag^+ ions inside the fibers ($2Ag + 2HI = 2Ag^+ + 2I^- + H_2$). The dissolution of Ag NWs was illustrated by the vanishing peaks of Ag NWs in X-ray powder diffraction (XRD) spectra and the absence of nanowires in SEM image (**Figure 3**A insert and Figure S8 in the Supporting Information), in contrast to XRD and SEM characterization of GGO-Ag NW composites before reduction (Supporting Information, Figure S7). With an increase of the Ag NWs fraction, the conductivities of the RGG-Ag fibers initially increase dramatically, and approach a plateau at about $9.1–9.3 \times 10^4$ S/m at 20 wt% of Ag NWs. This high conductivity of the Ag-doped graphene fibers, with an enhancement factor of 330%, is the record electrical conductivity for neat macroscopic CRG fibers and films.[7,14,17] Compared with the enhancement factors of doping graphene films, our result is about two-times higher than that of $AuCl_3$-doped graphene membranes (130%),[34] and comparable to that of nitric acid-doped stacked graphene films (≈300%).[35] The typical X-ray photoelectron spectroscopy (XPS) spectrum of reduced fibers with the maximum conductivity shows the existence of a small quantity of Ag as low as 0.05 Atom% (i.e., 500 ppm) (Supporting Information, Figure S10). The platform of conductivity further implies the molecular doping mechanism, which was observed in graphene films.[34,35] We pondered that the dissolved Ag+ ions in the reduction process are responsible for the in situ doping (Figure 3E).

As to the fibers reduced by VC, the Ag NWs keep their morphology and crystalline characteristics after the chemical reduction. The XRD pattern of VC-reduced graphene-Ag fibers shows four identical peaks of Ag NWs (*111, 200, 220, 311* facets) to the GGO-Ag NWs composite (Figure 3D).[36] The SEM images also distinctly illustrate the preservation of nanowires between graphene sheets interlayers, as indicated by the arrows in Figure 3B insert and Figure S9 in the Supporting Information. The conductivity of VC-reduced graphene fibers steadily increases from 8.1×10^3 S/m of neat graphene fiber to 2.2×10^4 S/m at 50 wt% Ag NW fraction (250% enhancement). Different from the conductivity evolution of HI-reduced samples, this steadily increasing conductivity implies a complexion mechanism for the VC-reduced fibers (Figure 3F).[37,38] Compared with the conductivity of HI-reduced Ag-doped graphene fibers, this relatively lower value of VC-reduced graphene fibers is possibly ascribed to their lower extent in restoring of conjugated lattice from original graphene oxide sheets,[14,31–33] which is demonstrated by the experimental result that VC-reduced neat graphene fibers show lower conductivity (8.1×10^3 S/m) than HI-reduced neat fibers (2.8×10^4 S/m).

The breakdown current density is a very important index to evaluate the current capacity of a certain electrical conductor. The HI-reduced neat graphene fibers have a relatively low maximum current density, 440 A/cm^2. After Ag doping, the breakdown current density of graphene fibers shows a considerable increasing (about 1500%) up to 7.1×10^3 A/cm^2 (**Figure 4**A), about 16 times higher than that of fibers of chemically reduced graphene nanoribbons.[39] By increasing the voltage to a certain level till the failure voltage value is reached, it was observed that the breakage of graphene fibers occurred as indicated by the flashing of red light. This phenomenon illustrates that resistive heating is the main failure mechanism.[40,41] SEM inspection of the broken section shows that the integrated graphene sheets become connected fragments at the tips due to the destruction of the excessive Joule heat (Figure 4B,C). The doping-induced enhancement in current capacity could be attributed to the improvement of electrical conductivity.[40] Although the current capacities of doped graphene fibers are much smaller

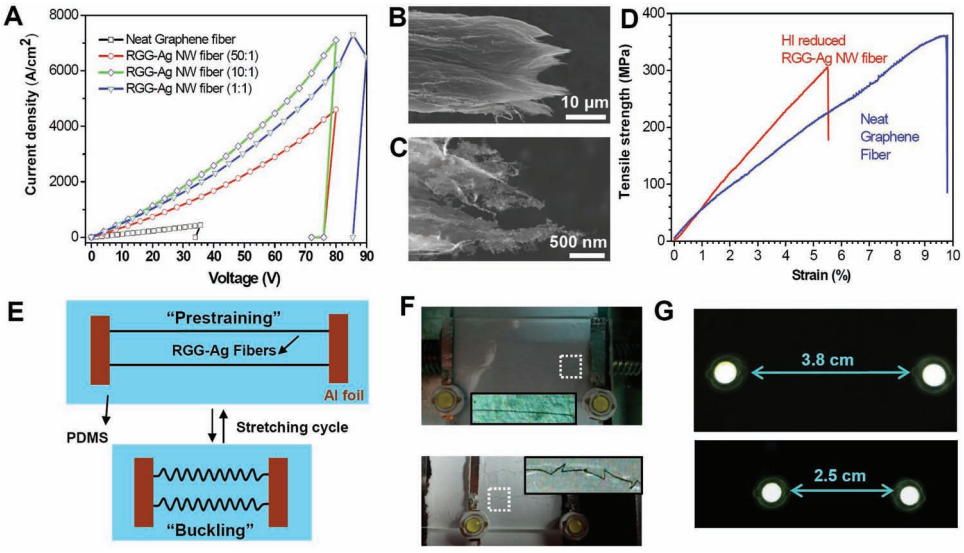

Figure 4. A) Measured current density as a function of voltage under electrical stressing of HI-reduced Ag-doped graphene fibers with various feed ratios of graphene to Ag NW. B,C) SEM images of the electrical failure tips of Ag-doped graphene fiber. D) Typical mechanical testing curves of neat graphene fiber and HI-reduced Ag-doped graphene fibers under tensile stressing. E) Schematic process of preparing stretchable RGG-Ag fiber array. F) The stretchable array constructed by RGG-Ag fibers in the stretched (top) and relaxed state (bottom). The inserted images are magnified photos of the RGG-Ag fibers in the respective areas indicated by the rectangles. G) The working states of RGG-Ag-fiber-based stretchable circuit in stretched (top) and relaxed state (bottom).

than pristine graphene sheets (10^7–10^8 A/cm^2),[40,41] further processing thermal annealing or graphitization should bring immense improvements in maximum current density to spun graphene fibers.

Stretchable Conductors of Ag-Doped Graphene Fibers: Mechanical tensile tests show that the HI-reduced RGG-Ag fibers are strong and flexible (Figure 4D). The neat RGG fibers without introduction of Ag NWs possess typical tensile strength of 360 MPa and a breakage tensile strain about 10%, similar to previous reports on spun RGG fibers without divalent-ion crosslinking.[14] Reduced fibres (RGG-Ag fibers) reduced from GGO-Ag NWs fibers containing 50 wt% Ag NWs showed typical strength of 305 MPa at ultimate strain of 5.5%, which is comparable to the strength of the filtrated CRG papers.[23] Compared with the neat RGG fibers, the decreasing strength and ultimate tensile strain for RGG-Ag fibers could be blamed for the introduction of voids originally occupied by Ag NWs.

Depending on their high conductivity and good mechanical performance, RGG-Ag fibers are proper candidates for use as flexible conductors. Using the prevalent prestraining-buckling approach to stretchable circuits,[42,43] we prepared stretchable array of RGG-Ag fibers (Figure 4F) on polydimethylsiloxane (PDMS) substrates (the process is depicted in Figure 4E). The RGG-Ag fibers are fixed to the Al foils by silver glue on the 150% prestrained PDMS substrate. Under compression in the fiber axis during the strain relaxation, the RGG-Ag fibers buckled to become curved threads without breakage, because of their good flexibility. The stretchable conductors made from RGG-Ag fibers can be safely stretched below 150% strain under electrical loading. As shown in Figure 4G and Figure S11 in the Supporting Information, the constructed circuit kept working after 150% stretching, indicating by the lightening LED chips, and the increasing length between the two LED chips further indicated the stretching process. After 50 cycles of stretching-relaxation, the circuit is still stretchable, as demonstrated by the invariable electrical resistance (Supporting Information, Figure S12). Additionally, the electrical conductivity of Ag-doped graphene fibers presented good stability in air, similar to the Au-doped graphene films.[34] The HI-reduced Ag-doped graphene fibers showed about 10% decrease in electrical conductivity after baking at 80 °C in air for two days, and the value became stable at 12% decrease in a further baking process for a longer time (Supporting Information, Figure S13). Compared with the initial conductivity of neat graphene fibers, the high conductivity of Ag-doping graphene fibers confirmed the fact that the Ag-doping still had considerable efficiency in enhancement of electrical conductivity.

In conclusion, we present a novel and scalable approach to highly conductive graphene-metal hybrid fibers by industrially viable wet-spinning of graphene oxide and commercial Ag nanowires, followed by chemical reduction. The Ag-doped/hybridized graphene fibers can be made continuously up to hundreds of meters long, and they show record electrical conductivity for chemically converted graphene materials, as well as highly enhanced current capacity. The fibers also possess excellent mechanical strength and flexibility. Such integrated merits guarantee the use of Ag-doped graphene fibers for the construction of stretchable circuits. The orientational order in graphene liquid crystals and the flow-induced alignment during fiber-spinning render both the graphene sheets and the Ag NWs with preferred alignment along the fiber axis, which favors continuous spinning, the effective enhancement of electrical conductivity, and the maintenance of the mechanical performance of the graphene fibers.

Experimental Section

Materials, preparation of GGO, and instruments sections are described in the Supporting Information.

Preparation of GGO-Ag NWs Spinning Dopes: From GGO aqueous dispersion,[11] we prepared GGO DMF dispersion by replacing water with DMF via a centrifugation process three times. The as-purchased Ag NWs dispersion was diluted to 1 mg/mL to quantitatively mix with the GGO DMF dispersions in a series of mass concentrations from 1% to 50%. The mixtures of GGO-Ag NWs were centrifugated to get GGO-Ag NWs gels, and DMF was added to prepare spinning dopes with a total concentration about 4 mg/mL after violent vibration in a vortex mixer.

Continuous Wet-Spinning of GGO-Ag NWs Fibers: Following the wet-spinning protocol and homemade apparatus depicted in Figure S4 in the Supporting Information, the GGO-Ag NWs spinning dopes were injected into an ethyl acetate coagulation bath (0.2 mL/min). The spun gel fibers were pulled out from the coagulation bath. After thermal drying, the continuous GGO-Ag NWs fibers were collected on a rotating plastic drum. Finally, the as-spun fibers were dried at 60 °C in air for 1 h and then dried at 60 °C under vacuum for 12 h, affording GGO-Ag NWs fibers.

Chemical Reduction for Fabrication of RGG-Ag Fibers: The dried GGO-Ag NWs fibers were immersed in HI (40%) or VC (0.1 M) aqueous solution, and the solution was heated to 90 °C and kept for 12 h. Then, the fibers were picked up from the reduction system, and rinsed by water and ethanol successively three times. The Ag-doped RGG fibers were obtained after vacuum drying at 100 °C for 12 h.

Fabrication of Stretchable Arrays of RGG-Ag Fibers: As illustrated in Figure 4E, the RGG-Ag fibers were aligned on the prestrained PDMS substrate (150% strain on uniaxial drawing stage), with two ends fixed on the Al foils by silver glue. Then, the fibers were coated with a thin layer of liquid PDMS resin to fix the fibers on the substrate. After baking at 100 °C for 12 h, the prestraining of PDMS was released and the RGG-Ag fibers buckled to form curved threads.

Supporting Information

Supporting information is available from the Wiley Online Library or from the author.

Acknowledgements

This work was supported by the National Natural Science Foundation of China (No. 51173162), the Qianjiang Talent Foundation of Zhejiang Province (No. 2010R10021), the Fundamental Research Funds for the Central Universities (No. 2013XZZX003), the Research Fund for the Doctoral Program of Higher Education of China (No. 20100101110049), and the Zhejiang Provincial Natural Science Foundation of China (No. R4110175).

Received: February 18, 2013
Revised: March 23, 2013
Published online: May 3, 2013

[1] C. N. R. Rao, A. K. Sood, K. S. Subrahmanyam, A. Govindaraj, *Angew. Chem., Int. Ed.* **2009**, *48*, 7752.
[2] M. J. Allen, V. C. Tung, R. B. Kaner, *Chem. Rev.* **2010**, *110*, 132.
[3] Q. Y. He, S. X. Wu, Z. Y. Yin, H. Zhang, *Chem. Sci.* **2012**, *3*, 1764.
[4] X. Huang, Z. Y. Yin, S. X. Wu, X. Y. Qi, Q. Y. He, Q. C. Zhang, Q. Y. Yan, F. Boey, H. Zhang, *Small* **2011**,*7*, 1876.
[5] X. Huang, Z. Y. Zeng, Z. X. Fan, J. Q. Liu, H. Zhang, *Adv. Mater.* **2012**, *24*, 5979.
[6] K. S. Novoselov, A. K. Geim, S. V. Morozov, D. Jiang, Y. Zhang, S. V. Dubonos, I. V. Grigorieva, A. A. Filrsov, *Science* **2004**, *306*, 666.
[7] Y. W. Zhu, S. Murali, W. W. Cai, X. S. Li, J. W. Suk, J. R. Potts, R. S. Ruoff, *Adv. Mater.* **2010**, *22*, 3906.
[8] H. Bai, C. Li, G. Q. Shi, *Adv. Mater.* **2011**, *23*, 1089.
[9] X. Huang, X. Y. Qi, F. Boey, H. Zhang, *Chem. Soc. Rev.* **2012**, *41*, 666.
[10] D. Q. Wu, F. Zhang, P. Liu, X. L. Feng, *Chem. Eur. J.* **2011**, *17*, 10804.
[11] D. R. Dreyer, S. Park, C. W. Bielawski, R. S. Ruoff, *Chem. Soc. Rev.* **2010**, *39*, 228.
[12] Z. Xu, C. Gao, *Nat. Commun.* **2011**,*2*, 571.
[13] Z. Xu, Y. Zhang, P. G. Li, C. Gao, *ACS Nano* **2012**, *6*, 7103–7113.
[14] Z. Xu, H. Y. Sun, X. L. Zhao, C. Gao, *Adv. Mater.* **2013**, *25*, 188.
[15] X. Z. Hu, Z. Xu, C. Gao, *Sci. Rep.* **2012**, *2*, 767.
[16] H. P. Cong, X. C. Ren, P. Wang, S. H. Yu, *Sci. Rep.* **2012**, *2*, 613.
[17] Z. L. Dong, C. C. Jiang, H. H. Cheng, Y. Zhao, G. Q. Shi, J. Lan, L. T. Qu, *Adv. Mater.* **2012**, *24*, 1856.
[18] Y. X. Xu, K. X. Sheng, C. Li, G. Q. Shi, *ACS Nano* **2010**, *4*, 4324.
[19] L. Estevez, A. Kelarakis, Q. M. Gong, E. H. Da'as, E. P. Giannelis, *J. Am. Chem. Soc.* **2011**, *133*, 6122.
[20] L. Qiu, J. Z. Liu, S. L. Y. Chang, Y. Z. Wu, D. Li, *Nat. Commun.* **2013**, *3*, 1241.
[21] H. Y. Sun, Z. Xu, C. Gao, *Adv. Mater.* **2013**, *25*, 2554.
[22] D. A. Dikin, S. Stankovich, E. J. Zimney, R. D. Piner, G. H. Dommett, G. Evmenenko, S. T. Nguyen, R. S. Ruoff, *Nature* **2007**, *448*, 457.
[23] H. Q. Chen, M. B. Müller, K. J. Gilmore, G. G. Wallace, D. Li, *Adv. Mater.* **2008**, *20*, 3557.
[24] W. S. Hummers, R. E. Offeman, *J. Am. Chem. Soc.* **1958**, *80*, 1339.
[25] Z. Xu, C. Gao, *ACS Nano* **2011**, *5*, 2908.
[26] J. E. Kim, T. H. Han, S. H. Lee, J. Y. Kim, C. W. Ahn, J. M. Yun, S. O. Kim, *Angew. Chem., Int. Ed.* **2011**, *50*, 3043.
[27] B. Dan, N. Behabtu, A. Martinez, J. S. Evans, D. V. Kosynkin, J. M. Tour, M. Pasquali, I. I. Smalyukh, *Soft Matt.* **2011**, *7*, 11154.
[28] S. H. Aboutalebi, M. M. Gudarzi, Q. B. Zheng, J. K. Kim, *Adv. Funct. Mater.* **2011**, *21*, 2978.
[29] F. Guo, F. Kim, T. H. Han, V. B. Shenoy, J. X. Huang, R. H. Hurt, *ACS Nano* **2011**, *5*, 8019.
[30] H. Ko, V. V. Tsukruk, *Nano Lett.* **2006**, *6*, 1443.
[31] S. F. Pei, J. P. Zhao, J. H. Du, W. C. Ren, H. M. Cheng, *Carbon* **2010**, *48*, 4466.
[32] M. J. Fernáedez-Merino, L. Guardia, J. I. Paredes, S. Villar-Rodil, P. Solís-Fernández, A. Martínez-Alonso, J. M. D. Tascón, *J. Phys. Chem. C* **2010**, *114*, 6426.
[33] W. F. Chen, L. F. Yan, *Nanoscale* **2011**, *3*, 3132.
[34] K. K. Kim, A. Reina, Y. M. Shi, H Park, L. J. Li, Y. H. Lee, J. Kong, *Nanotechnology* **2010**, *21*, 285205.
[35] A. Kasry, M. A. Kuroda, G. J. Martyna, G. S. Tulevski, A. A. Bol, *ACS Nano* **2010**, *4*, 3839.
[36] C. Gao, W. W. Li, Y. Z. Jin, H. Kong, *Nanotechnology* **2006**, *17*, 2882.
[37] K. Y. Chun, Y. Oh, J. Rho, J. H. Ahn, Y. J. Kim, H. R. Choi, S. Baik, *Nat. Nanotechnol.* **2010**, *5*, 853.
[38] I. N. Kholmanov, C. W. Magnuson, A. E. Aliev, H. F. Li, B. Zhang, J. W. Suk, L. L. Zhang, T. Peng, S. H. Mousavi, A. B. Khanikaev, R. Piner, G. Shvets, R. S. Ruoff, *Nano Lett.* **2012**, *12*, 5679.
[39] E. Y. Jang, J. Carretero-González, A. Choi, W. J. Kim, M. E. Kozlov, T. Kim, T. J. Kang, S. J. Baek, D. W. Kim, Y. W. Park, R. H. Baughman, Y. H. Kim, *Nanotechnology* **2012**, *23*, 235601.
[40] R. Murali, Y. Yang, K. Brenner, T. Beck, J. D. Meindl, *Appl. Phys. Lett.* **2009**, *94*, 243114.
[41] K. J. Lee, A. P. Chandrakasan, J. Kong, *IEEE Electron Device Lett.* **2011**, *32*, 557.
[42] M. Zu, Q. W. Li, G. J. Wang, J. H. Byun, T. W. Chou, *Adv. Funct. Mater.* **2013**, *23*, 789.
[43] D. J. Lipomi, M. Vosgueritchian, B. C. K. Tee, S. L. Gellstrom, J. A. Lee, C. H. Fox, Z. N. Bao, *Nat. Nanotechnol.* **2011**, *6*, 788.